Automated 3D Segmentation of Vertebral Bodies and Intervertebral Discs from MRI

Aleš Neubert*, Jurgen Fripp, Kaikai Shen, Olivier Salvado
The Australian E-Health Research Centre
CSIRO ICT Centre
Brisbane, Australia
Email: ales.neubert@csiro.au

Raphael Schwarz, Lars Lauer
Siemens Healthcare
Erlangen, Germany

Craig Engstrom and Stuart Crozier
School of Human Movement Studies,
*School of Information Technology and Electrical Engineering
The University of Queensland
Brisbane, Australia

***Abstract*—Recent developments in high resolution MRI scanning of the human spine are providing increasing opportunities for the development of accurate automated approaches for pathoanatomical assessment of intervertebral discs and vertebrae. We are developing a fully automated 3D segmentation approach for MRI scans of the human spine based on statistical shape analysis and template matching of grey level intensity profiles. The algorithm reported in the present study was validated on a dataset of high resolution volumetric scans of lower thoracic and lumbar spine obtained on a 3T scanner using the relatively new 3D SPACE (T2-weighted) pulse sequence, and on a dataset of axial T1-weighted scans of lumbar spine obtained on a 1.5T system. A 3D spine curve is initially extracted and used to position the statistical shape models for final segmentation. Initial validating experiments show promising results on both MRI datasets.**

***Index Terms*—Spine Imaging, Image Segmentation, MRI, Statistical Shape Models**

I. Introduction

Recently MR pulse sequences such as 3D Sampling Perfection with Application optimised Contrasts using different flip angle Evolution (SPACE) have been developed that provide detailed high-quality 3D images of the human spine with spatial resolutions comparable to CT [1]. Given the superior soft tissue contrast offered by MRI and the ongoing improvements of new pulse sequences for high resolution imaging of the vertebral column, MRI will likely play an increasing role in the radiological assessment of acute and chronic disorders of the human vertebral column.

The aim of our research is to develop an automated system for accurate detection, segmentation and morphological assessment of the vertebral bodies (VBs) and intervertebral discs (IVDs) to facilitate the diagnosis and treatment planning of common pathological conditions of the spine. Potentially, an automated segmentation approach offers many benefits over time- and expertise-intensive manual segmentation procedures particularly for analyses of large, high-resolution volumetric imaging studies within both clinical and applied research environments. The challenges facing the development of an automated analysis system include intrinsic anatomical factors such as the accurate identification of the geometrically complex bony vertebral elements, the non-linear alignment and intimate interlocking of various bony and soft-tissue structures, intra- and inter-patient variations within and across the local regions and entire extent of the vertebral column as well as MR artifacts such as signal inhomogeneities, low signal-to-noise (SNR) or contrast-to-noise (CNR) ratio. Furthermore, advanced image processing and segmentation techniques are required to provide robust and precise analysis for MRI images of various contrast, different quality of acquisition and spatial resolution.

II. Previous Work

CT provides high contrast resolution between the bony vertebrae and surrounding soft tissues, making it possible to exploit the image gradient information or other edge detection-based algorithms for segmentation procedures [2]. While CT images are useful to assess the vertebrae [3] their use in systems for computer-aided diagnosis of IVD pathologies is however limited by relatively reduced visualisation of soft tissues compared with MRI. The capacity for MRI to provide high contrast images of the IVDs along with good visualisation of the bony vertebrae is an attractive feature of this imaging modality, however most current studies are acquired with anisotropic resolution making it challenging for volumetric segmentation in 3D. Hence previous segmentation approaches (both for vertebrae and IVDs) have been based on 2D analysis, typically based on images obtained in the sagittal plane. Hough transform or edge detectors figure among the most common methods of IVD detection [4]. These techniques can provide good initial information about the location of the vertebrae and the IVDs in the spine [5] but are usually insufficient to provide final segmentation results. In [6], the results of an edge detection technique (opening by reconstruction operator) are further refined using a trained classifier based on statistical texture features. Open active contours (snakes) are used in [5] to detect landmarks at disc approximate edges and the landmarks are used to drive a 2D segmentation of the cervical IVDs by active shape model in the central sagittal cross-section. The 2D segmentation process is then spread in both sagittal directions and the final 3D volume is obtained by combining the segmentations from all slices. An analogy to brain segmentation is presented by [7] who segment the IVDs

978-0-7695-4588-2/11 $26.00 © 2011 IEEE
DOI 10.1109/DICTA.2011.12

of the lumbar spine in the central sagittal cross-section by a combination of a fuzzy c-means segmentation algorithm, to reduce the partial volume effects, and a prior knowledge from a probabilistic disc atlas.

Adapted edge detecting techniques have also been used to segment the VBs from MRI, such as successive ellipses fitting to horizontal cross-sections [8] which are then combined to generate a final 3D volume. Authors in [9] segment successive 2D sagittal slices using iterative normalised cuts. A 3D segmentation procedure has been proposed by [10] using statistical shape models of VBs and the spinal cord. The shape is deformed using contours extracted by the Canny edge detector together with vectors of geometric attributes.

All of the above mentioned techniques (with the exception of [10]) rely on two-dimensional image data, are often specific to particular MRI contrast or need some manual input from the user. However, with recent MRI techniques making acquisition of high resolution data possible, there is a great potential for analysing the anatomical structures in further details utilising all the 3D information provided. Moreover, a fully automated approach would enable analysis of larger datasets that would provide results for robust statistical testing.

In our research, we develop a fully automatic 3D segmentation algorithm for both the VBs and IVDs of all spine areas (lumbar, thoracic, cervical) that can be applied to MRI images of different contrast and spatial resolution. The segmentation method is based on 3D statistical shape model (SSM) analysis and grey level profile (GLP) registration. The automatic procedure is initialised by object-recognition analysis of the sagittal cross-sections followed by an automatic search for the 3D spine curve. Centre points of the VBs and IVDs are determined from an intensity profile along this spine curve. We demonstrate the potential of this approach on datasets comprising scans of the lumbar and thoracic areas with different slice thickness and MRI contrast.

III. Method

A. Image Database and Pre-Processing

Three datasets (Table I) were used in this study to validate our segmentation algorithm. The first dataset consists of T1-weighted (T1w) axial scans of the lumbar spine of six healthy subjects with relatively high slice thickness (5-6mm), in-plane resolution 0.3-0.4mm (parameters common in clinical practise). The second and third dataset contain high resolution T2-weighted (T2w) 3D SPACE scans of lumbar (dataset II) and lower-thoracic (dataset III) areas from six healthy subjects. The 3D SPACE pulse sequence at 3T has shown a good potential for clinical assessment and diagnosis [1], [11] and has the advantage of 3D volumetric acquisition providing high-resolution images with superior spatial resolution and level of details (axial slice thickness 1-1.2mm, in-plane resolution 0.34x0.34mm). Example axial and sagittal slices of images from the three datasets are shown in Fig. 1.

To minimise the noise while preserving edge information, images were smoothed by gradient anisotropic diffusion (15 iterations with time step 0.01 and conductivity 0.25).

TABLE I
Image Datasets
(L - Lumbar Area, T - Thoracic Area)

	Modality	Area	# Scans	# VBs	# IVDs	Slice Resolution	Slice Thickness
I	T1w	L	6	11	11	0.3-0.4mm	5-6mm
II	T2w	L	6	30	29	0.34mm	1-1.2mm
III	T2w	T	6	27	26	0.34mm	1-1.2mm

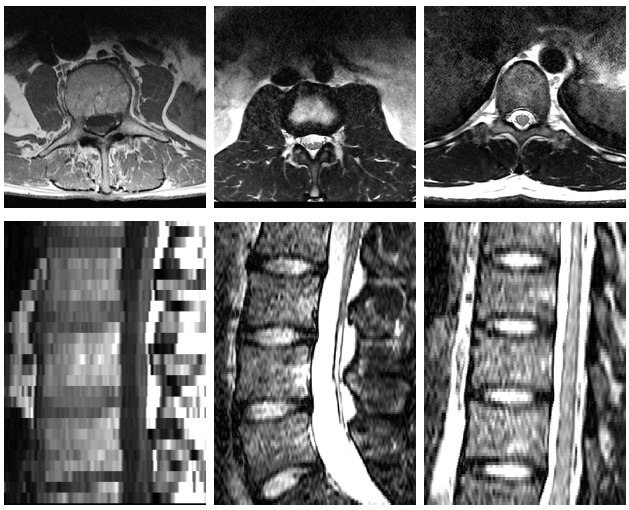

Fig. 1. Example Axial and Sagittal Cross-sections. One subject from each dataset is presented in each column (see Table I - lumbar T1w on the left, lumbar T2w in the middle and thoracic T2w on the right). Partial voluming effect can be observed for images of dataset I due to the larger slice thickness (bottom-left).

Each database was manually segmented providing a set of 11 lumbar VBs (L1-L5) and 11 lumbar IVDs (T12L1-L4L5) for the first dataset of T1w images, a set of 30 lumbar VBs and 29 lumbar IVDs (second dataset) and 27 thoracic (T8-T12) VBs and 26 thoracic IVDs (T7T8-T11T12) for the third dataset. We used the manually segmented volumes to create 6 three-dimensional SSMs (one VB and IVD per dataset). The procedure for generating SSMs is described in the next section.

B. Model Creation and Optimisation

Each manually segmented volume (VBs, IVDs) was transformed into a triangular mesh by applying the marching cubes algorithm and parameterised using SPHARM [12]. Subsequently, the optimization procedure presented in [13] was used to generate the SSM.

As a result of the marching cubes algorithm, each shape is represented as a triangular mesh with a variable number of vertices and facets. The key problem to create a 3D SSM is to find a corresponding representation of all the meshes, ie. with the same number of points that spatially correspond to each other across the database. Supposing we have such a database of corresponding meshes $\boldsymbol{x_i}, i = 1, \ldots, N$, we can then Procrustes align them and define a point distribution for each of the vertices. Their mean positions $\bar{x}$ (thus introducing

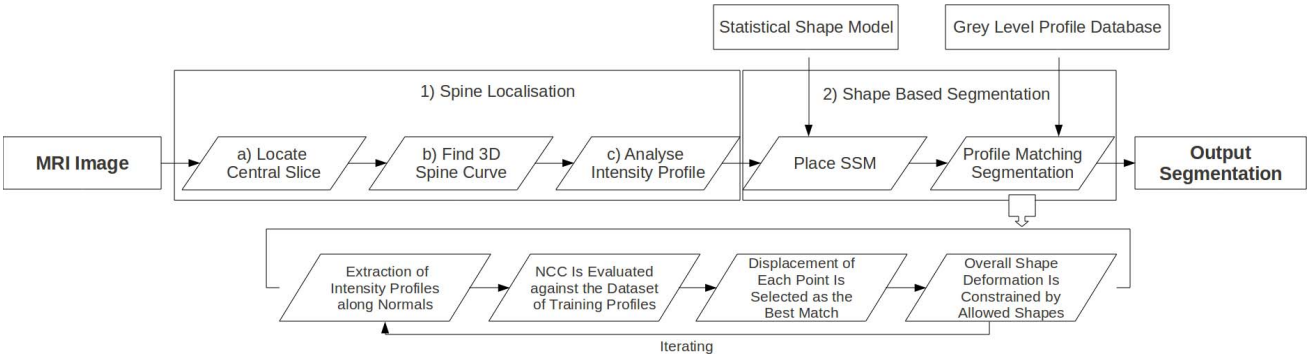

Fig. 2. Segmentation Algorithm Pipeline. The segmentation procedure consists of several step. After the pre-processing, the spine location and approximate positions of VBs and IVDs are found. The statistical mean shape is placed into the found locations and refined by grey level profile matching.

a 'mean shape') and covariance matrix C can be computed as described in Eq. 1:

$$\bar{\boldsymbol{x}} = \frac{1}{N}\sum_{i=1}^{N}\boldsymbol{x_i},\ C = \frac{1}{N-1}\sum_{i=1}^{N}(\boldsymbol{x_i}-\bar{\boldsymbol{x}})(\boldsymbol{x_i}-\bar{\boldsymbol{x}})^T \quad (1)$$

Each eigenvector of the covariance matrix describes a mode of variation of the dataset and the corresponding eigenvalue $\lambda_i, i = 1,\ldots,N$ its importance. By taking the largest n eigenvalues (where $n \leq N$ and the eigenvalues are sorted in descending order in absolute value), a ratio of $(\sum_{i=1}^{n}|\lambda_i| / \sum_{i=1}^{N}|\lambda_i|)$ of the total variance can be captured by using the subset of n modes of variation while reducing the computational cost when using all N modes. New shapes $\boldsymbol{x}$ can be generated by weighting each mode of variation and adding it to the mean shape (Eq. 2):

$$\boldsymbol{x} = \bar{\boldsymbol{x}} + \boldsymbol{P}\boldsymbol{b}, \quad (2)$$

where $\boldsymbol{P}$ is the matrix of first n orthonormal modes of variation (eigenvectors of C) and $\boldsymbol{b} = (b_1,\ldots,b_n)$ is the vector of weights that influences each mode of variation [14]. We define an allowed shape as a shape whose mode parameters (weights $\boldsymbol{b}$) lie within 3 standard deviations of each mode. The allowed shapes are then used for the segmentation.

For the purpose of finding point-wise corresponding meshes, an inhouse implementation of the optimisation algorithm [13] is used. The process of finding point-wise correspondences is formulated as an otimisation problem of finding the best shape re-parametrisation across the dataset. Initially, all shapes are mapped to a unit sphere using the explicit parametric representation of [12]. The sphere representation is more tractable to re-parametrisation by moving, deleting, interpolating and resampling the points on its surface [15]. Further improvement in speed is suggested in [13] by unfolding the sphere into a 2D square via mapping to octahedron and by performing these operations in the plane. The optimisation criteria is inspired from the theory of signal encoding. A SSM is thought as a shape (mesh) with modes of variation of each point. Every shape in the database is then described (encoded) as a weighted sum of these modes of variation (as in Eq. 2). The weights $\boldsymbol{b} = (b_1,\ldots,b_n)$ describe the distance from the model shape. The optimal parametrisation problem is then formulated as finding the simplest shape that is capable to adequately describe (encode) the shapes in the dataset with the fewest modes of variations. More details can be found in [15].

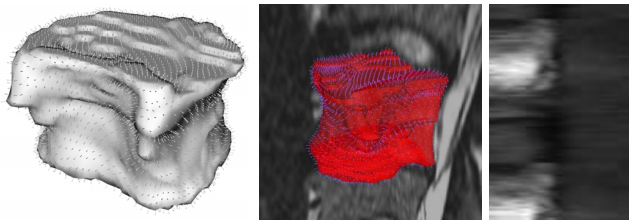

Fig. 3. Extraction of the Grey Level Profiles. Surface normals at each point are cumputed (panel a) and intensities are extracted from the MRI image (panel b) along these normals at points uniformly sampled in both outside and inside areas. An excerpt from a GLP is shown in panel c) where each horizontal line represents a GLP of one surface point. Intensities from outside of the shown VB are in the left half, intensities extracted from the inside of the VB are in the right half of the profiles.

Once the optimal parametrisation of all shapes have been found, a database of 1D grey level profiles is extracted from MRI images for each shape at all surface points. The profiles are extracted along the normal of each point using cubic BSpline interpolation. This image information is used to drive the shape deformation during the segmentation procedure.

The validation experiments were performed on the same databased the models were created on but for each segmented VB or IVD, its shape and profile were removed from the model (leave-one-out strategy).

C. Segmentation Algorithm Pipeline

The segmentation procedure consists of several processing steps that are described in Fig. 2. The spine curve is found to determine the spine coordinate system, which is needed in order to place the SSMs into the intial positions before they are deformed to obtain the final segmentations results. The successive steps of the process are described in this section

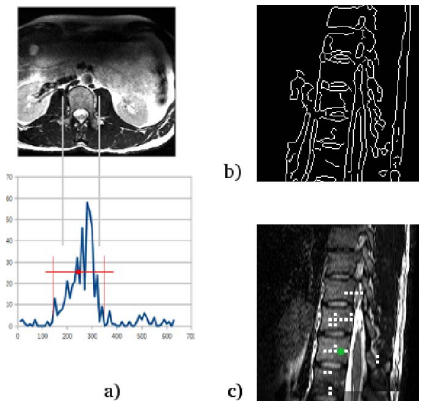

Fig. 4. Scoring of Sagittal Cross-sections. On the left (panel a) is the graph of scores of respective sagittal slices, aligned with a lumbar axial slice. The central cross-section with most of the VBs and IVDs can be determined. The result of Canny edge detection on the central sagittal slice is shown at panel b) and the corresponding slice with points of high correlations with the vertebrae template are shown on the panel c). The green circle identifies the found seed for spine curve extraction.

(following the chart in Fig. 2).

1) Spine Localisation: Initially, approximate locations of all visible VBs and IVDs are found. The spine localisation is performed in several steps. First, we detect a central sagittal section, ie. the sagittal cross-section passing closest to most centres of VBs and IVDs (Section a). Second, a 3D spine curve passing through centres of VBs and IVDs is extracted. This is achieved by analysing each axial cross-section and finding a line of axial vertebral symmetry in each slice. The algorithm was presented by [16] and is described in Section b). Last, the approximate centres of VBs and IVDs are localised in the 3D spine curve by analysing the intensity profile along the found spine curve (Section c).

a) Locate the Central Sagittal Cross-section
The central sagittal cross-section (ie. passing closest to centres of most vertebral bodies) was identified at first by correlating the Canny edge detector results on the extracted sagittal slices with an artificial model of two adjacent vertebrae and an ellipse-like IVD. The number of points with the correlation coefficient over a selected threshold (empirically 0.35) was used to count a score of each slice. The median of the high score area is then chosen as the central sagittal cross-section (Fig. 4).

b) Find the 3D Spine Curve
The obtained central sagittal slice is used to initialise a search for a 3D spine curve described in [16]. The mean coronal and axial coordinates of points of highest correlation within the template are used as a seed point. A line of axial symmetry for each axial cross-section is found by maximising a similarity measure (mutual information) and the centre of the VB or IVD is refined along this line using an operator finding centres of circular structures [16]. A robust 3D fitting of 3rd degree polynomials in each coordinate direction is performed to find the continuous spine curve in three dimensions (see Fig. 5).

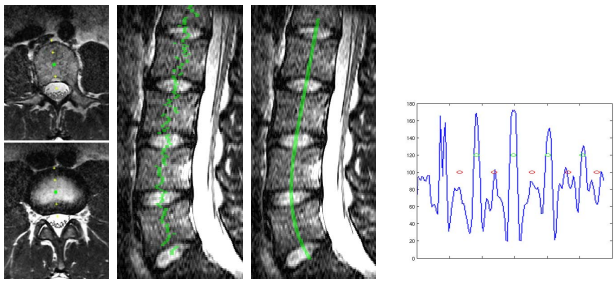

Fig. 5. Extraction of the 3D Spine Curve. Example axial slices with found lines of axial symmetry and approximate centres of respective VB or IVD (green dots) are shown in panel a). The centres are projected into the middle sagittal cross-section in panel b) and the fitted polynomial spine curve is shown in panel c). Intensity profile along this curve is extracted (panel d) and used to find the number of imaged VBs and IVDs and their centres in 3D (red dots for centres of VBs and green dots for centres of IVDs).

c) Analyse the Intensity Profile Along the Curve
The intensity profile along the spine curve is analysed to find approximate centre positions of the VBs and IVDs where the shape models for segmentation would be placed. Points of high gradient, where anatomical borders are likely to occur, are searched and the obtained segments are length-analysed to identify either an IVD (length between 4-15mm) or a VB (15-37mm). Longer segments are split into regions of VB and IVD following the same assumptions of average anatomy dimensions. The ranges are chosen to accommodate a majority of adult population while clearly distinguishing between an IVD and a VB An example result is presented in Fig. 5d.

Knowing the approximate positions of VBs and IVDs centres, their boundaries along the spine curve in 3D and their axial orientation, we can place the statistical mean shapes from our SSMs into these locations. The segmentation process is finalised by deforming these shapes to precisely match the segmented anatomies. The procedure is describe in the next section.

2) Shape Base Segmentation: As a result of the SSM creation, every manual segmentation in the training database is represented as a 3D triangular mesh with the same number of points that spatially correspond to each other along the dataset. Thus, for each manually segmented case, MRI image intensities (GLPs) along the mesh point normals can be extracted and saved for all the cases (Fig. 3). The GLPs are extracted from both the interior and the exterior of the VB or IVD and centred at the mesh point itself. The length of the training profiles in this study was 61 points (30 inside the shape, 30 ouside plus the edge point) with the spacing of 0.25mm. The database of GLPs (training profiles) from all the manually segmented cases is used to drive the iterative deformation process. The statistical mean shape with mesh points spatially corresponding to mesh points of the manual segmentations are placed to initial positions (found in previous

TABLE II
DICE SCORES FOR SEGMENTATION RESULTS

Dataset	Anatomy	#VBs or #IVDs	Mean	Median	StdDev
I	VB	11	0.83	0.82	0.03
II	VB	30	0.85	0.87	0.08
III	VB	27	0.87	0.88	0.05
I	IVD	11	0.78	0.79	0.07
II	IVD	29	0.76	0.76	0.07
III	IVD	26	0.80	0.83	0.07

section).

At each iteration (we used 10 iterations in this study), the optimal displacement of each shape point is sought after (Fig 2). First, grey level profiles are extracted along normals of the current shape. These normals are double the length of the training profiles. A set of possible displacements is defined independently for each point along its normal (points where the grey level profiles were extracted). For each possible displacements, the normalised cross-correlation of the GLP around the new position is evaluated against each corresponding training profile in the database. The best match is selected as the new point position. The overall shape deformation is then constrained to lie within 3 standard deviations of the modes of variation of the SSM (the space of allowed deformations).

IV. RESULTS

The mean shape models and the primary modes of variation of the VBs and IVDs are shown in Fig. 6. In the case of the VB from dataset I (Fig. 6, upper left section), the most important mode of variation explains primarily the variation in vertical dimension of the VBs. The high variation in the height of the VBs is partially a consequence of the relatively large axial slice thickness (5-6mm) and the resulting partial volume effect. High variations in the SSM of VBs from the second dataset (Fig. 6 bottom left section) can be observed in areas of the vertebral pedicles. This variation is partially due to inconsistency in the manually segmented contours and partially due to significant differences among the anatomies of thoracic vertebrae in this area.

The accuracy of the automated segmentation was validated by computing the Dice score similarity measure (Eq. 3) between the results of our automated algorithm (volume A) and the manual segmentations (volume M):

$$Dice(A, M) = 2\frac{|A \cap M|}{|A| + |M|} \quad (3)$$

The results are reported in Table II, the segmentation process is illustrated in Fig. 7 and example segmentation results are shown in Fig. 8.

As can be seen from the Table II the results for lumbar and thoracic VB are very good. The slight decrease in the results in the thoracic and particularly the lumbar IVDs is still being

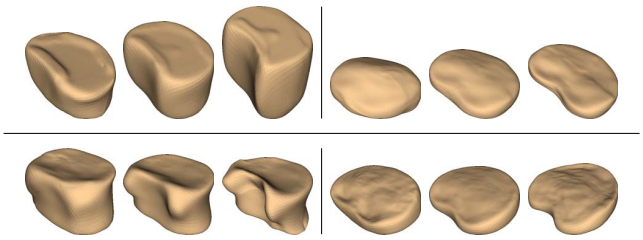

Fig. 6. Mean shapes (in the middle) and their first mode of variation (-3 StdDev on the left, +3 StdDev on the right) of two VBs (left) and two IVDs (right). First column corresponds to the first dataset (T1w), second column to the third dataset (T2w SPACE, thoracic area).

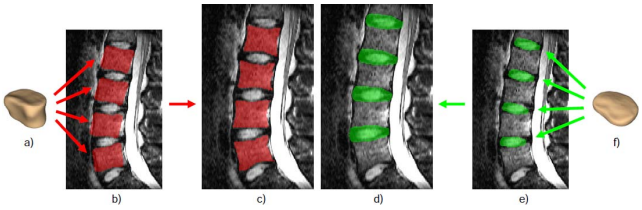

Fig. 7. Example Result Image with Segmented VBs and IVDs. The middle slice of an example lumbar T2w 3D SPACE image is shown. The mean shapes (panels a and f) are placed to found initial positions (panels b and e) and deformed following the process described in Fig. 2. The final segmentation results are shown on panels c and d.

investigated. One of the observed problems occuring for the T2w images is the attraction of the IVDs towards the high gradient edges of the spinal nerves in the spinal cord (Fig. 8, bottom right).

Imperfections in dataset I are likely due to the partial voluming effect. Because of the bigger voxel size in the superior-inferior direction, the interface between a VB and an IVD is less clearly defined and any single one voxel misalignment in this direction contributes importantly to the Dice score (especially for the IVDs that are only 3-4 voxels thick) (see Fig. 8, left column). However, the overall results appear satisfactory given the level of details captured in images of such resolution.

V. CONCLUSION

Shape based segmentation has become a widely used strategy to constrain difficult segmentation problems in many MRI-based studies. Our study shows its potential for automated spine anatomy segmentation in the thoracic and lumbar regions when high-resolution MRI data are acquired as well as for data with larger slice thickness that are commonly used in current clinical practice. The method can be used on MRI scans of the thoracic and lumbar spine with different contrast and acquisition parameters providing a dataset with manual segmentations is available.

Both quantitative and visual evaluations demonstrate promising results and usability on most cases, however further improvements to achieve good results on most images and more extensive validations on a larger dataset are needed. Our upcoming aim is to acquire a larger dataset of spine images

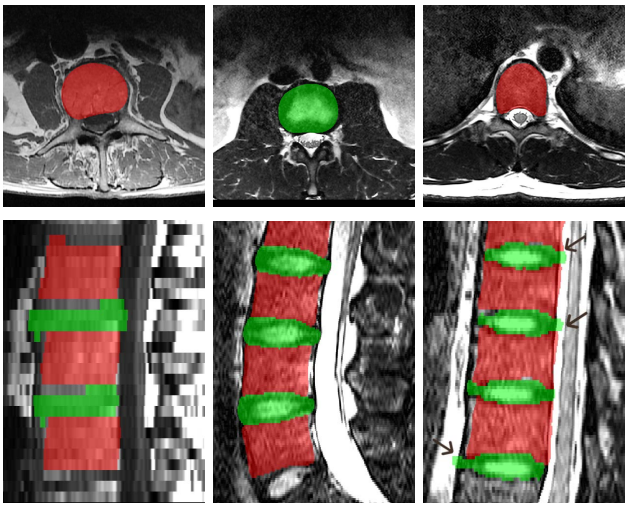

Fig. 8. Example Results from the Three Datasets. The same slices as in Fig. 1 with overlaid segmentation results are presented. Arrows in the bottom-right slice indicates areas of imprecise segmentation.

to enable generation of more specific models (ie. specialised model for each vertebra). These models, across all regions of the spine, will capture individual anatomical variations in more detail. Additionally, further improvements in the segmentation results will be undertaken by incorporating multi-shape models into connected templates of anatomical variations and by improving the spine localisation by a more robust and generic spine curve search algorithm. A study showing the sensitivity of the approach to precise initialisation will also be conducted.

REFERENCES

[1] T. Meindl, S. Wirth, S. Weckbach, O. Dietrich, M. Reiser, and S. O. Schoenberg, "Magnetic resonance imaging of the cervical spine: comparison of 2D T2-weighted turbo spin echo, 2D T2*weighted gradient-recalled echo and 3D T2-weighted variable flip-angle turbo spin echo sequences." *European radiology*, vol. 19, no. 3, pp. 713–21, 2009.

[2] J. Ma, L. Le, Y. Zhan, X. Zhou, M. Salganicoff, and A. Krishnan, "Hierarchical Segmentation and Identification of Thoracic Vertebra Using Learning-Based Edge Detection and Coarse-to-Fine Deformable Model," in *International Conference on Medical Image Computing and Computer Assisted Intervention*, 2010, pp. 19–27.

[3] T. Klinder, J. Ostermann, M. Ehm, A. Franz, R. Kneser, and C. Lorenz, "Automated model-based vertebra detection, identification, and segmentation in CT images," *Medical image analysis*, vol. 13, no. 3, pp. 471–82, 2009.

[4] R. Shi, D. Sun, Z. Qiu, and K. L. Weiss, "An Efficient Method for Segmentation of MRI Spine Images," in *IEEE: International Conference on Complex Medical Engineering*, 2007, pp. 713–717.

[5] S. Seifert, I. Wachter, G. Schmelzle, and R. Dillmann, "A knowledge-based approach to soft tissue reconstruction of the cervical spine," *IEEE transactions on medical imaging*, vol. 28, no. 4, pp. 494–507, 2009.

[6] C. Chevrefils, F. Chériet, C.-E. Aubin, and G. Grimard, "Texture analysis for automatic segmentation of intervertebral disks of scoliotic spines from MR images," *IEEE transactions on information technology in biomedicine*, vol. 13, no. 4, pp. 608–20, 2009.

[7] S. K. Michopoulou, L. Costaridou, E. Panagiotopoulos, R. Speller, G. Panayiotakis, and A. Todd-Pokropek, "Atlas-based segmentation of degenerated lumbar intervertebral discs from MR images of the spine," *IEEE transactions on bio-medical engineering*, vol. 56, no. 9, pp. 2225–31, 2009.

[8] A. K. Jerebko, G. P. Schmidt, X. Zhou, J. Bi, V. Anand, J. Liu, S. Schoenberg, I. Schmuecking, B. Kiefer, and A. Krishnan, "Robust parametric modeling approach based on domain knowledge for computer aided detection of vertebrae column metastases in MRI," in *IPMI'07: Proceedings of the 20th international conference on Information processing in medical imaging*, 2007, pp. 713–724.

[9] S.-H. Huang, Y.-H. Chu, S.-H. Lai, and C. L. Novak, "Learning-based vertebra detection and iterative normalized-cut segmentation for spinal MRI," *IEEE transactions on medical imaging*, vol. 28, no. 10, pp. 1595–605, 2009.

[10] C. Davatzikos, D. Liu, D. Shen, and E. H. Herskovits, "Spatial normalization of spine MR images for statistical correlation of lesions with clinical symptoms," *Radiology*, vol. 224, no. 3, pp. 919–26, Sep. 2002.

[11] M. P. Lichy, B. M. Wietek, J. P. Mugler, W. Horger, M. I. Menzel, A. Anastasiadis, K. Siegmann, T. Niemeyer, A. Königsrainer, B. Kiefer, F. Schick, C. D. Claussen, and H.-P. Schlemmer, "Magnetic resonance imaging of the body trunk using a single-slab, 3-dimensional, T2-weighted turbo-spin-echo sequence with high sampling efficiency (SPACE) for high spatial resolution imaging: initial clinical experiences." *Investigative Radiology*, vol. 40, no. 12, pp. 754–760, 2005.

[12] C. Brechbühler, G. Gerig, and O. Kübler, "Parametrization of Closed Surfaces for 3-D Shape Description," *Computer Vision and Image Understanding*, vol. 61, no. 2, pp. 154–170, 1995.

[13] R. H. Davies, C. J. Twining, and C. Taylor, "Groupwise surface correspondence by optimization: representation and regularization," *Medical image analysis*, vol. 12, no. 6, pp. 787–96, 2008.

[14] T. Cootes, C. Taylor, D. Cooper, J. Graham, and Others, "Active shape models-their training and application," *Computer vision and image understanding*, vol. 61, no. 1, pp. 38–59, 1995.

[15] R. H. Davies, C. J. Twining, T. F. Cootes, J. Waterton, and C. Taylor, *3D Statistical Shape Models Using Direct Optimisation of Description Length*, ser. Lecture Notes in Computer Science, 2002, vol. 2352, pp. 1–17.

[16] T. Vrtovec, S. Ourselin, L. Gomes, B. Likar, and F. Pernuš, "Automated generation of curved planar reformations from MR images of the spine," *Physics in Medicine and Biology*, vol. 52, no. 10, pp. 2865–2878, 2007.